Asynchronous Access Mechanism for Deterministic Converged 5G and Time-Sensitive Networks

Jiamin Cui, Jiacheng Li, Yongxiang Zhao, Chunxi Li, Zonghui Li, *Member, IEEE*, Kang G. Shin, *Life Fellow, IEEE*, and Bo Ai, *Fellow, IEEE*

***Abstract*—As required by Industry 4.0, industry is now moving towards flexible and customizable manufacturing. To succeed in this transition, the convergence of 5th Generation Mobile Communication Technology (5G) and Time-Sensitive Networks (TSNs) is a key enabler and has thus attracted significant interest from industry and standardization groups. However, the end-to-end (e2e) delay and jitter of time-critical flows will get exacerbated if the transmission opportunities are missed in the TSN part due to the 5G transmission jitter and the clock skew between the two component networks. To mitigate this problem, we propose a novel asynchronous access mechanism (AAM) that isolates the jitter only in the 5G system and ensures no transmission jitter in the TSN. We then exploit AAM to develop an asynchronous traffic scheduling model (ATSM) for coordinated allocation of resources in the 5G and TSN systems. Extensive OMNeT++ simulations demonstrate that AAM effectively isolates TSN-side jitter and that ATSM efficiently coordinates resource allocation across the 5GS and TSN domains.**

***Index Terms*—e2e, traffic scheduling, asynchronous access, deterministic transmission, jitter isolation, TSN, 5G.**

I. Introduction

MORE and more industrial use cases require deterministic communication to enable production automation [1], [2], such as the control of cooperating robots [3] and Automated Guided Vehicles (AGVs) [4]. Real-time networks serve as the foundation for providing deterministic and reliable transmission for such industrial time-sensitive communication. According to the prevalent transmission media, industrial real-time networks can be characterized as a combination of wired and wireless networks.

Current industrial real-time networks are still dominated by wired technologies [5] such as CAN, PROFIBUS, EtherCAT, and TTEthernet. However, these technologies either provide low data rates [6] or are manufacturer-specific, thereby making them incompatible with each other [7]. Consequently, IEEE 802.1 Time-Sensitive Networking (TSN) [8], which defines a variety of mechanisms such as time synchronization and traffic shaping to guarantee deterministic transmission, has been a promising solution for future unified industrial networks in the wired environment [9].

However, such a wired technology is only suitable for production facilities that are static and have long life cycles [10] thus lacking the flexibility and modularity [11], [12] required by Industry 4.0. Industry and academia have therefore turned to wireless technologies to achieve this goal [10], [13]. The 5th generation mobile communication technology (5G), which has supported industrial use cases from its inception, is considered as a key technology for Industry 4.0. Specifically, its ultra-reliable low-latency communication (URLLC) feature provides a flexible frame structure and faster signaling to support the low-latency communication required by intelligent manufacturing [14].

In the Industry 4.0 vision, both static, long-life-cycle facilities and flexible equipment, such as robots, reconfigurable machinery, and mobile industrial devices, are highly connected [15]. This vision requires the convergence of wireless 5G and wired TSN communication in factories [16]. A deterministic periodic flow generates packets periodically, each of which must reach its receiver within a given deadline. Such flows are a common industrial traffic class [15]. This paper focuses on deterministic periodic flows from 5G user equipment (UE) to servers in the TSN domain. For example, in a hot-rolling process, sensors distributed along the rolling line periodically collect vibration data and deliver them through 5G to a server in the TSN domain, enabling timely feedback for slab-thickness control.

The 3rd Generation Partnership Project (3GPP) has specified an integration architecture between the 5G System (5GS) and TSN in [17]. In this architecture, the 5GS is logically represented as one or more TSN transparent bridges, enabling wireless devices to be connected to a wired TSN network. The interworking between 5GS and TSN is realized through TSN Translators, namely the Device-Side TSN Translator (DS-TT) on the UE side and the Network-Side TSN Translator (NW-TT) associated with the User Plane Function (UPF) [16].

However, such an integration of 5GS and TSN may significantly exacerbate the end-to end (e2e) delay and jitter of periodic flows from a 5G UE to a destination in TSN [18], [19].

Received 5 February 2026; revised 29 July 2026; accepted 12 September 2026. Date of publication 16 September 2026; date of current version 5 November 2026. This work was supported in part by the National Natural Science Foundation of China under Grant 62531003 and Grant 62272034 and in part by the Science and Technology Project of State Grid Corporation of China under Grant 52120025003R-295-LZ. Recommended for acceptance by W. Wang. *(Corresponding author: Zonghui Li.)*

Jiamin Cui and Zonghui Li are with the School of Computer Science and Technology, Beijing Jiaotong University, Beijing 100044, China (e-mail: jiamincui@bjtu.edu.cn; lizonghui@bjtu.edu.cn).

Jiacheng Li, Yongxiang Zhao, Chunxi Li, and Bo Ai are with the School of Electronic and Information Engineering,Beijing Jiaotong University, Beijing 100044, China (e-mail: 21120075@bjtu.edu.cn; yxzhao@bjtu.edu.cn; chxli1@bjtu.edu.cn; boai@bjtu.edu.cn).

Kang G. Shin is with the Department of Electrical Engineering and Computer Science, University of Michigan, Ann Arbor, MI 48109 USA (e-mail: kgshin@umich.edu).

Digital Object Identifier 10.1109/TMC.2026.3734470

1536-1233 © 2026 IEEE. All rights reserved, including rights for text and data mining, and training of artificial intelligence and similar technologies. Personal use is permitted, but republication/redistribution requires IEEE permission. See https://www.ieee.org/publications/rights/index.html for more information.

Authorized licensed use limited to: University of Michigan Library. Downloaded on November 23,2026 at 18:04:37 UTC from IEEE Xplore. Restrictions apply.

First, assuming TSN employs the time-aware shaper (TAS), each packet from 5GS must arrive at the gateway (GW) before the start of its "prepared" transmission opportunity in TSN, which we call the *time-triggered (TT) access mechanism* (TAM). The transmission opportunities are configured via the gate control list (GCL) of TAS and repeat periodically with the flow period. Second, it is difficult for 5GS to successfully deliver a packet before the start of its transmission opportunity owing to the following factors [19]: (a) high transmission delay in the radio interface due to poor radio channel conditions; (b) high queueing delay in the transmission buffer (before transmitting via radio interface); (c) the packet arriving at the UE contains errors and must be retransmitted; (d) the clock skew between 5GS and TSN. Thus, if a packet output by 5GS misses its transmission opportunity in TSN, the packet has to wait for the opportunity assigned to the next packet. Missing a transmission opportunity will enlarge the e2e delay and jitter significantly.

To mitigate the enlargement of delay and jitter, we propose a novel *asynchronous access mechanism* (AAM) to bridge 5GS and TSN. AAM is not a new time-synchronization protocol. Rather, it is an access and scheduling mechanism that provides redundant transmission opportunities in the TSN for each 5G packet, thereby reducing the waiting time due to missed transmission opportunities. Furthermore, AAM holds the packet at the last TSN hop to shape its TSN residence time to a fixed constant. As a result, AAM decouples the transmission interaction between 5GS and TSN. This robustness is achieved at the cost of additional TSN transmission opportunities, hence requiring coordinated cross-domain resource allocation to prevent uncontrolled resource consumption. We then build an e2e *asynchronous traffic scheduling model* (ATSM) to allocate the resources of TSN and 5GS. Finally, we validate the performance of AAM and ATSM by simulation on OMNeT++ [20].

The remainder of this paper is organized as follows. Section II discusses the related work while Section III describes the delay and jitter enlargement under TAM and mitigates it with the AAM. Section IV proposes the ATSM based on the AAM. Section V evaluates the performance of the AAM and ATSM. Finally, Section VI concludes this paper.

II. Related Work

3GPP defined the integration architecture of 5GS and TSN in Release-16 and Release-17 [17]. Such an architecture has motivated research on traffic scheduling for the converged network of 5GS and TSN. Singhal et al. [21] present 5GS resource allocation in next-generation broadband wireless access networks. Integrating TSN, Adil et al. [16] present a comprehensive survey on e2e traffic scheduling of 5G-TSN networks. These scheduling approaches can be treated as either separate or joint scheduling depending on whether the resources in the two networks are allocated cooperatively or not.

A. Separate Scheduling on 5G-TSN Networks

In the case of separate scheduling, the e2e delay requirement of a time-critical flow is first divided into 5GS and TSN delay budgets, and then the two networks schedule their own network resources independently according to their assigned budgets. Larrañaga et al. [22] scheduled multiple resource blocks (RBs) for multiple packets of time-critical flows to solve the periodic resource conflicts in 5GS. Cai et al. [23] and Silva et al. [24] dynamically mapped the QoS requirements obtained from time-sensitive communication assistance information (TSCAI) to 5G QoS Identifier (5QI), and added dynamic RBs to pre-allocated RBs if the latter was insufficient for data transmission. Yang et al. [25] scheduled enhanced mobile broadband (eMBB) and URLLC traffic, aiming to improve eMBB throughput while satisfying the delay requirements of URLLC traffic, based on QoS information obtained from TSCAI. These works allocate resources within 5GS under a given 5GS delay budget, without considering coordinated delay-budget allocation between TSN and 5GS.

B. Joint Scheduling on 5G-TSN Networks

Joint scheduling requires 5GS and TSN to belong to the same operator. Compared to separate scheduling, it does not allocate fixed delay budgets to the two domains before resource allocation. Instead, it treats the e2e delay requirement as a unified constraint and coordinates the resource allocation of 5GS and TSN accordingly. This enables the scheduler to adjust the delay–resource tradeoff between the two domains according to the traffic demand and network configuration. Wang et al. [26] proposed a unified scheduling model to allocate appropriate time slots for time-critical flows using the cyclic queuing and forwarding (CQF) mechanism and proposed a reinforcement learning-based algorithm to search for the optimal scheduling solution. Li et al. [27] maintained the freshness of information by scheduling sampling and transmission decisions cooperatively to reduce energy consumption. Ginthör et al. [11] showed that the flow patterns from TSN to 5GS have a significant impact on capacity and delay in 5GS, and Ginthr et al. [28] proposed an e2e optimized scheduling framework to jointly schedule resources across the two network systems.

All these works depended on the assumption that under the time synchronization between 5GS and TSN, packet transmission from the 5GS never missed the transmission opportunity in TSN. However, the assumption does not always hold due to the randomness, interference and synchronization error in the 5GS. As a result, the transmission interaction between 5GS and TSN may result in the delay and jitter enlargement as mentioned in Section I. To mitigate this problem, we propose the AAM, which enables deterministic communication in converged 5GS and TSN even under asynchronous conditions. Furthermore, we propose the ATSM based on the AAM to coordinate the allocation of 5GS and TSN resources.

III. Asynchronous Access Mechanism

We first present the application scenario and then explain the problem of increased e2e delay and jitter in the context of TAM. Finally, the basic ideas and implementation of AAM are detailed to mitigate this problem.

Authorized licensed use limited to: University of Michigan Library. Downloaded on November 23,2026 at 18:04:37 UTC from IEEE Xplore. Restrictions apply.

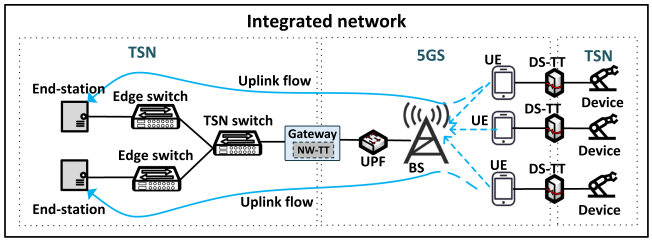

Fig. 1. The converged network that integrates 5GS and TSN.

A. Application Scenario

Fig. 1 shows a scenario in which 5GS is integrated with TSN as a logical bridge, as defined by 3GPP [17]. The DS-TT and NW-TT enable interworking between 5GS and TSN. The gateway (GW) switch hosts the NW-TT function and serves as the boundary between the 5GS and the TSN network. Thus, no separate NW-TT to GW link or additional inter-device delay is introduced. The TSN switch connected to the end station (ES) is called the edge switch. All flows originate from the TSN device on the right-hand side of Fig. 1 and are delivered to end stations (ESs) on the left-hand side. All ESs are attached through TSN switches, thereby supporting TSN forwarding and time synchronization in the wired domain. These flows are all TT flows. Specifically, the source of a TT flow periodically generates fixed-length packets. Each TT flow is subject to the e2e delay requirement for packet delivery. Since the path segment consisting of the TSN device, DS-TT and UE is an exclusive path, the transmission delay on this segment is assumed to be constant. We refer to the source of each TT flow as UE in the following analysis.

Additionally, we assume that the clocks in TSN and 5GS are synchronous within their respective domains but can be asynchronous across domains. Under AAM, both the GW and the edge switch retain TAS and provide periodic transmission slots. We also assume that 5GS adopts the frequency division duplex (FDD) scheme where downlink and uplink transmissions use different frequency bands. This assumption simplifies the presentation of uplink resource allocation but is not fundamental to AAM. For a time division duplex (TDD) deployment, the offset and duration of each 5GS transmission instance must be constrained such that all of its occupied TTIs fall within the configured uplink symbols or slots. The resource-capacity and OFDMA non-overlap constraints are then applied only to these feasible uplink resources. Therefore, extending our work to TDD does not require a new framework. A single base station (BS) serves all UEs, meaning that one uplink carrier is shared among them.

B. Delay and Jitter Enlargement

In our work, the integration of 5GS and TSN refers to the use of TAS in TSN to reserve a transmission opportunity for each packet of a TT flow on every link along its route. We present an example in Fig. 2 to show the enlargement problem of e2e delay and jitter in such an integration of 5GS and TSN. The numerical values in Fig. 2 are illustrative but not intended to represent realistic delay characteristics for wireless and wired links. In Fig. 2(a)–(d), the UE in 5GS sends a packet every 100 ms to the ES in TSN via the GW and edge switch. Fig. 2(a) and (b) show the enlargement of e2e delay and jitter caused by the clock skew between 5GS and TSN, and the 5G transmission jitter, respectively.

As shown in Fig. 2(a), in an ideal situation — i.e., there is neither 5G transmission jitter nor clock skew between 5GS and TSN — the GW and edge switch reserve a transmission opportunity every 100 ms (= the flow period) on their output ports, which is shown as black hollow circles, and the black dashed arrows depict the ideal transmission processes. Each packet experiences a constant delay of 45 ms and the e2e jitter of 0. However, considering the clock skew between the two systems, the packets may arrive at TSN earlier (depicted by the blue line) or later (depicted by the red line) from the perspective of TSN. We set the clock skew between 5GS and TSN to 10 ms, i.e., the clock of TSN may be at most 10 ms earlier or later than that of 5GS. The value of clock skew depends on the synchronization implementation, deployment environment, and hardware/software characteristics. 10 ms is used only as an illustrative timing mismatch to make the amplification effect visible in Fig. 2(c). On the one hand, packet #1 arrives 10 ms earlier than the prepared transmission opportunity and has to wait for it, leading to the actual e2e delay of 55 ms. On the other hand, packet #2 arrives 10 ms later than the prepared transmission opportunity and must wait for the opportunity in the next period, leading to the actual e2e delay of 135 ms. If the arrival time is arbitrarily close to but still later than the reserved transmission opportunity, the waiting time at the GW may approach one full flow period, namely, the worst case. Thus, the experienced e2e delay can be as low as 45 ms and as large as 145 ms (wait at GW for 100 ms), creating a jitter of 100 ms which equals the flow period. Thus, a small skew between the clocks of the two systems may lead to a significantly larger e2e delay and jitter than scheduled.

Similarly, as shown in Fig. 2(b), we assume that the clocks are synchronized, the delay budget in 5GS is estimated to be the average delay over a period of time, and the transmission opportunities prepared by TSN are scheduled by reserving the delay budget of 5GS. The transmission jitter of 5GS is 10 ms, meaning packets may arrive at most 10 ms earlier or later than the ideal arrival time calculated by the delay budget. In the ideal situation shown by the black dashed arrows, each packet experiences a constant delay of 55 ms and the e2e jitter of 0. Packet #1 arrives at the GW earlier and experiences an e2e delay of 55 ms, including a waiting delay of 10 ms. Packet #2 arrives later and must wait 90 ms for the next transmission opportunity, resulting in an e2e delay of 155 ms. The resulting jitter is 100 ms, equal to the flow period. Therefore, a small 5G transmission jitter may also lead to a significantly larger e2e delay and jitter than scheduled.

In fact, the e2e delay and jitter enlargement are caused by missing TSN transmission opportunities. To mitigate this problem, we propose the AAM that decouples the interaction between 5GS and TSN transmissions.

Authorized licensed use limited to: University of Michigan Library. Downloaded on November 23,2026 at 18:04:37 UTC from IEEE Xplore. Restrictions apply.

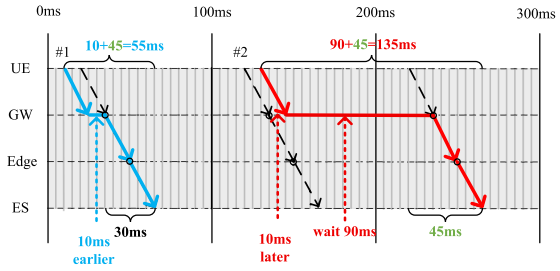

(a) Issue caused by clock skew.

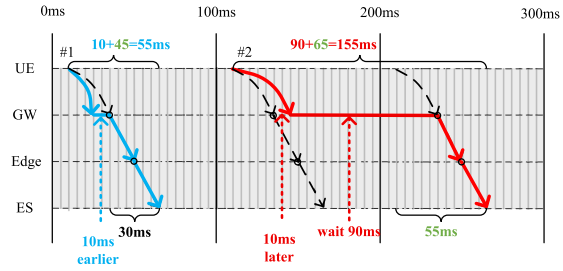

(b) Issue caused by the 5G transmission jitter.

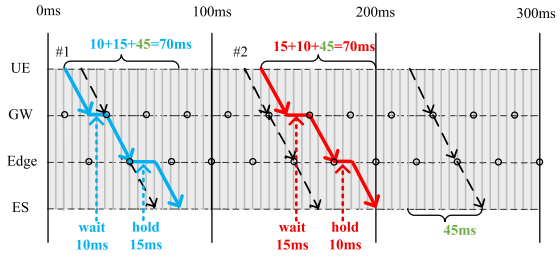

(c) AAM solution to the issue in (a).

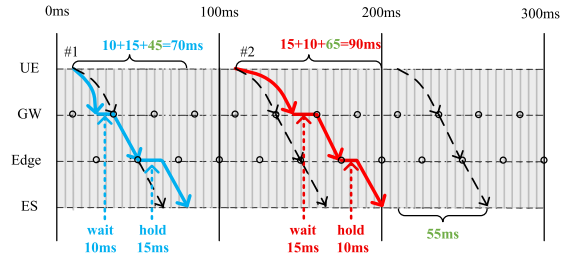

(d) AAM solution to the issue in (b).

Fig. 2. (a) and (b) show that a small clock skew between 5GS and TSN and 5G transmission jitter will lead to a large amplification of the residence time and jitter in TSN. (c) and (d) show that AAM can keep the residence time of TSN as a constant and eliminate such an amplification.

C. Basic Ideas of the AAM

The AAM has two basic components: (1) over-provisioning transmission opportunities to reduce packet waiting time at the GW and (2) holding packets at the edge switch to maintain a constant residence time in TSN.

First, TSN over-provisions transmission opportunities for each TT flow to reduce its waiting time at the GW. The period of these opportunities for flow f_i is denoted by T_i. As shown in Fig. 2(c), the UE sends a packet every 100 ms, whereas the GW provides a TSN transmission opportunity every $T_i = 25$ ms. The GW therefore provides four potential opportunities per packet and uses the first one available after the packet arrives. In this way, the maximum waiting time at the GW is reduced from 100 ms to 25 ms. However, only one of the four opportunities carries a packet, while the other three constitute resource overhead. Thus, reducing T_i decreases the waiting-time bound at the cost of additional unused opportunities.

After being forwarded from the GW, a packet reaches the edge switch at the corresponding gate-opening instant. The edge switch then performs the AAM holding operation instead of immediately forwarding the packet. Let T_i be the period of the over-provisioned TSN transmission opportunities, which may be smaller than the flow period, as will be discussed later. As shown in Fig. 2(c), $T_i = 25$ ms. Packets #1 and #2 experience similar transmission processes: (1) waiting at the GW, (2) transmission from the GW to the edge switch, (3) holding at the edge switch, and (4) transmission from the edge switch to the ES, and the corresponding delays are denoted as $f_i.wait$, $D^{TSN}_{i,(1)}$, $f_i.hold$ and $D^{TSN}_{i,(2)}$. The delay in TSN can be represented as:

$$D^{TSN}_i = f_i.wait + D^{TSN}_{i,(1)} + f_i.hold + D^{TSN}_{i,(2)}, \quad (1)$$

where $D^{TSN}_{i,(1)}$ and $D^{TSN}_{i,(2)}$ are constant under a deterministic TSN schedule. Because $f_i.wait \in [0, T_i)$, the holding time compensates for the waiting time such that their sum equals T_i, i.e., $f_i.wait + f_i.hold = T_i$. As can be seen from Fig. 2(c), packet #1 waits at the GW for 10 ms and is held at the edge switch for 15 ms, and packet #2 waits at the GW for 15 ms and is held at the edge switch only for 10 ms. This way, the residence time of each packet in TSN is fixed and can be represented as:

$$D^{TSN}_i = T_i + D^{TSN}_{i,(1)} + D^{TSN}_{i,(2)}. \quad (2)$$

Consequently, all packets of the flow experience the same TSN delay, regardless of when they are delivered by 5GS. This fixed residence time decouples the transmissions in the two domains, thereby mitigating the delay and jitter enlargement. As shown in Fig. 2(c), both packets experience the same e2e delay of 70 ms regardless of the clock skew between the two network systems. T_i must be selected such that $D^{TSN}_i = T_i + D^{TSN}_{i,(1)} + D^{TSN}_{i,(2)} \leq f_i.d$ according to (2). $f_i.d$ denotes the e2e delay requirement of f_i. Some periodic control applications require the e2e delay to be no larger than the flow period because each update must arrive before the next one is generated [6]. Similarly, Fig. 2(d) illustrates how the AAM can help mitigate the issues presented in Fig. 2(b). Moreover, the e2e jitter is confined to the 5GS component and is not amplified in the TSN domain.

The parameter T_i must, therefore, be selected carefully to balance TSN resource overhead against the e2e delay of the converged network.

- T_i enables a trade-off between the cost of TSN transmission opportunities and the transmission delay in TSN. According to (2), a smaller T_i leads to a lower TSN delay but increases the number of unused transmission opportunities for a flow, as shown in Fig. 2(a) and (c).

Authorized licensed use limited to: University of Michigan Library. Downloaded on November 23,2026 at 18:04:37 UTC from IEEE Xplore. Restrictions apply.

Algorithm 1: AAM at the GW.

1 function onReceivingPacketFrom5GS($f_i.packet$):
2 $f_i.buffer = f_i.packet.getPayload()$;
3 $f_i.receivedTime = now()$;
4 function onTransmissionOpportunity($f_i.timer$):
5 $resetTimer(f_i.timer)$;
6 **if** $f_i.buffer$ *is empty* **then**
7 return;
8 **else**
9 new $f_i.packet$;
10 $f_i.packet.setPayload(f_i.buffer)$;
11: $f_i.packet.setWait(now() - f_i.receivedTime)$;
12 send($f_i.packet$);
13 $f_i.buffer.reset()$;
14 **end**

Algorithm 2: AAM at the edge switch.

1 function onReceivingPacket($f_i.packet$):
2 delay($T_i - f_i.packet.getWait()$);
3 send($f_i.packet$);

- T_i balances the delay budgets in 5GS and TSN. The e2e delay consists of 5GS and TSN components:

$$D_i^{e2e} = D_i^{5GS} + D_i^{TSN} = D_i^{5GS} + T_i + D_{i,(1)}^{TSN} + D_{i,(2)}^{TSN}. \quad (3)$$

Given a fixed e2e delay requirement, decreasing T_i enlarges the delay budget available to 5GS and may reduce the number of frequency-domain RBs used by TT flows, but it also increases the number of redundant TSN transmission opportunities. Conversely, increasing T_i reduces the TSN resource overhead but tightens the 5GS delay budget and may require additional frequency-domain RBs. ATSM explicitly optimizes this cross-domain trade-off by jointly determining T_i, the TSN transmission offsets, the 5GS transmission duration, and the subchannel allocation under a unified e2e delay constraint, rather than assigning fixed delay budgets to the two domains in advance. The details are presented in Section IV.

It is, therefore, necessary to establish a comprehensive model to jointly schedule the resources of 5GS and TSN when the AAM is applied. This will be discussed in Section IV.

D. Implementation of the AAM

The AAM is composed of the following two parts.

- The GW caches a received packet of f_i until the next transmission opportunity, attaches the waiting time $f_i.wait$, and sends it toward the destination.
- The edge switch holds the packet of f_i for a duration of $f_i.hold$ and then delivers it to the final destination, where $f_i.hold + f_i.wait = T_i$.

The implementation details in the GW and the edge switch are described in Algorithms 1 and 2, respectively.

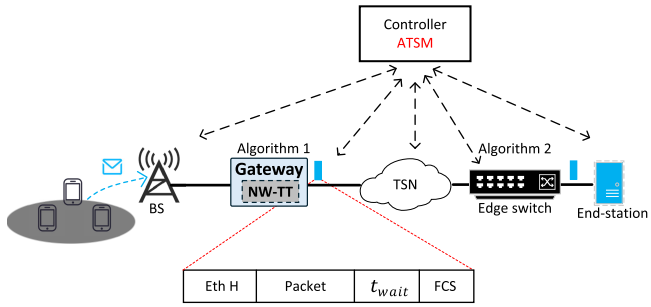

Fig. 3. An example of the deployment of the AAM.

In Algorithm 1, there are two functions in the GW. In the first function onReceivingPacketFrom5GS($f_i.packet$), once the packet of flow f_i is received, the GW caches the packet in the buffer $f_i.buffer$ prepared for this flow (Line 2). If there is already a packet in the buffer, the old packet will be replaced by the new packet. Then, the reception time of the packet is recorded (Line 3). In the second function onTransmissionOpportunity ($f_i.timer_i$), the function takes a timer as an input parameter. Since a timer is set for each flow f_i to trigger its transmission, the function first resets the timer for the next transmission opportunity for this flow (Line 5). It then checks whether the buffer of this flow is empty. On the one hand, the function does nothing if the corresponding buffer is empty. On the other hand, it attaches the waiting time to this packet and sends it before clearing the buffer if the buffer is not empty (Lines 6-13). The packet is forwarded only through the first available TSN transmission opportunity after its arrival; if no packet has arrived, the corresponding opportunity remains unused. This caching and forwarding operation enforces the inter-domain causality between 5GS and TSN. Consequently, ATSM does not require a conventional fixed constraint forcing a TSN transmission offset to occur after the scheduled 5GS completion time. The reserved TSN opportunities are potential opportunities rather than packet-specific transmissions, and the GW selects the first usable opportunity only after the packet has actually been received. Because these opportunities repeat every T_i, the runtime waiting time satisfies $0 \leq f_i.wait < T_i$; the term T_i in the e2e delay constraint, therefore, provides its deterministic upper bound.

There is only one function in Algorithm 2. When the edge switch receives the packet $f_i.packet$, it holds the packet for $T_i - f_i.packet.getWait()$ which is consistent with the process mentioned before (Line 2). The packet is then delivered to the destination after the delay (Line 3).

As shown in Fig. 3, AAM can be easily integrated into the 5GS-TSN architecture proposed in [17]. The base station complies with the 5G network standard. Algorithm 1 and 2 are implemented in GW and edge switch, respectively. The GW stamps the packet waiting time into the packet payload and the edge switch extracts the waiting time from the received packets. The ATSM is implemented in the controller, whose detailed structure can be found from [17]. The controller collects the state of the converged network and the requirements of the flows, and

Authorized licensed use limited to: University of Michigan Library. Downloaded on November 23,2026 at 18:04:37 UTC from IEEE Xplore. Restrictions apply.

then calculates the configuration parameters of 5GS, TSN, GW and the edge switch using ATSM.

IV. Asynchronous Traffic Scheduling Model

We now formulate ATSM for scheduling resources in the AAM-based converged network. We first define the network and traffic models, then derive the network constraints and objective function, and finally transform the scheduling problem into an integer linear programming (ILP) problem.

A. Network and Traffic Models

The wired TSN network is defined as an undirected graph $G(V, E)$, where V is the set of nodes such as ESs, GW, and TSN switches, and E is the set of physical full-duplex links in TSN. Specifically, each physical link contains two dataflow links [29]. Let L^{TSN} denote the set of dataflow links in TSN, then we have:

$$\forall v_1, v_2 \in V, (v_1, v_2) \in E : [v_1, v_2], [v_2, v_1] \in L^{TSN}, \quad (4)$$

where (v_1, v_2) denotes the physical link between nodes v_1 and v_2, $[v_1, v_2]$ and $[v_2, v_1]$ are the corresponding directed dataflow links.

The set of dataflow links in 5GS is denoted by L^{5GS}. The entire set of dataflow links in the converged network can then be represented as $L = L^{TSN} \cup L^{5GS}$.

Let F be the set of flows. Each flow $f_i \in F$ is represented by the tuple:

$$\forall f_i \in F :< f_i.p, f_i.l, f_i.d >, \quad (5)$$

where $f_i.p$, $f_i.l$, and $f_i.d$ denote the period, packet length, and e2e deadline of the flow, respectively.

For each flow, we assume that only one packet is delivered in each period. The traffic generation rate is fully determined by the packet length and the period, i.e., $f_i.l/f_i.p$. Under AAM, the reserved TSN transmission-opportunity period T_i may be smaller than $f_i.p$. This creates redundant potential opportunities to absorb asynchronous arrivals but does not change the actual packet-generation rate. The datapath is determined in advance:

$$\forall f_i \in F : p_i = [l_1, l_2, \ldots, l_{h_i}], l_j \in L, \quad (6)$$

where h_i is the number of hops for f_i, p_i denotes the datapath for flow f_i. Table I summarizes the main notations/symbols used in this paper.

B. Scheduling Model

We formally define the transmission opportunities reserved in TSN and 5GS as potential transmission instances.[1] Let f_i^l denote the potential transmission instance of flow f_i on the dataflow link l.

[1]Since each transmission opportunity is allocated to an actually transmitted packet in the traditional traffic scheduling model of TSN, each transmission opportunity is also called a transmission instance [30]. However, in the AAM context, not every transmission opportunity corresponds to an actually transmitted packet. So, we extend the concept of transmission instances to potential transmission instances.

TABLE I
Notations Used in This Work

Symbol	Description
G	Wired TSN network
V	Set of nodes in TSN
E	Set of wired links in TSN
F	Set of all flows
L, L^{TSN}, L^{5GS}	Dataflow links of the whole network, TSN, and 5GS
$v_i \in V$	TSN node i
$(v_1, v_2) \in E$	Physical link between nodes v_1 and v_2
$[v_1, v_2], [v_2, v_1] \in L^{TSN}$	Dataflow links between nodes v_1 and v_2
$f_i \in F$	Flow i
p_i	Route of flow f_i
h_i	Number of hops of route p_i
T_i	Reserved TSN transmission period for f_i
$f_i.p$	Period of flow f_i
$f_i.l$	Frame length of f_i
$f_i.d$	End-to-end delay requirement of f_i
f_i^l	Transmission instance of f_i on link l
$f_i^l.T$	Transmission period of f_i^l
$f_i^l.o$	Start offset of f_i^l
$f_i^l.s$	Transmission delay of f_i^l
$\mathcal{F}$	Set of frequency-domain subchannel indices
$k, k_{\max}$	Subchannel index and number of available subchannels
$\mathrm{RB}_{t,k}$	RB occupying TTI t and subchannel k
$x_{i,k}^l$	Subchannel k on link l assigned to flow f_i
y_k^l	Subchannel k on link l assigned to any flow
$minP$	Minimum TSN-supported period
T_{TSN}	TSN hyperperiod
T_{5GS}	5GS hyperperiod

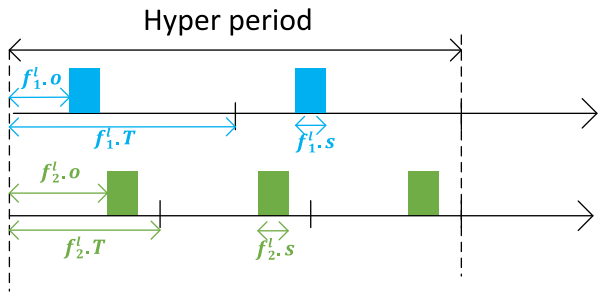

Fig. 4. Scheduling example in TSN.

1) Scheduling Model in TSN: In TSN, the potential transmission instance f_i^l is fully determined by the following triple:

$$\forall f_i \in F, \forall l \in p_i \cap L^{TSN} :$$
$$f_i^l = \{f_i^l.T, f_i^l.o, f_i^l.s\} \quad (7)$$

where $f_i^l.T$ denotes the period of the transmission opportunities reserved for f_i on the dataflow link l. $f_i^l.o$ and $f_i^l.s$ denote the offset and the transmission duration on dataflow link l, respectively. Fig. 4 shows an example.

For a single flow, $f_i^l.T$ is the same along its route (denoted as T_i) and $f_i^l.s$ is the ratio of the packet length to the link rate which is known a priori, and the pattern repeats in every cycle. For multiple flows, the pattern similarly repeats in every "hyper

Authorized licensed use limited to: University of Michigan Library. Downloaded on November 23,2026 at 18:04:37 UTC from IEEE Xplore. Restrictions apply.

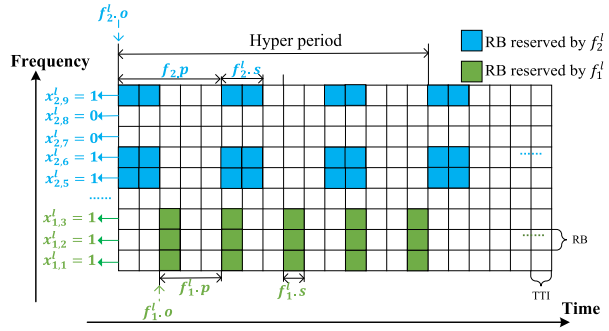

Fig. 5. Scheduling example in 5GS.

period". TSN's hyperperiod is defined as the least common multiple (LCM) of the periods of every flow's potential transmission instances:

$$T_{TSN} = LCM(\{T_i | f_i \in F\}). \tag{8}$$

As shown in Fig. 4, the reference zero points of all potential transmission instances of all flows are the same. In one hyperperiod, the potential transmission instance of f_1 on dataflow link l appears twice while that of f_2 appears thrice. $f_i^l.T$ and $f_i^l.o$ for all flows on TSN dataflow links along its route $l \in p_i \cap L^{TSN}$ (except for the last dataflow link) are variables.

2) Scheduling Model in 5GS: As shown in Fig. 5, the 5GS radio-resource grid has both time and frequency dimensions. We define $RB_{t,k}$ as the minimum allocation unit that occupies one TTI t in the time domain and one subchannel k in the frequency domain. We assume that the network operator has implemented a network slice that provides $k_{\max}$ subchannels in every TTI, which can be denoted as $\mathcal{F} = \{1, 2, \ldots, k_{\max}\}$. In the 5GS, semi-persistent scheduling (SPS) is adopted to support periodic traffic by reserving radio resources in a periodic manner [31]. Under SPS, transmission resources for initial packet transmissions are preconfigured and reused across periods. To reduce scheduling complexity, we assume that each potential transmission instance in 5GS can only occupy consecutive TTIs and we do not impose additional constraints on the frequency domain. In Fig. 5, there are two TT flows represented by blue and green colors. A potential transmission instance of f_1 and f_2 requires 3 and 6 blocks of transmission, respectively. A potential transmission instance of f_2 occupies two consecutive TTIs.

The potential transmission instance in 5GS can thus be identified by the following variables:

$$\forall f_i \in F, \forall l \in p_i \cap L^{5GS}:$$

$$f_i^l = \{f_i.p, f_i^l.o, f_i^l.s, x_i^l\} \tag{9}$$

$$x_i^l = \{x_{i,k}^l | k \in \mathcal{F}\} \tag{10}$$

where $f_i.p$ is the flow period and $x_{i,k}^l$ is a binary variable equal to 1 if subchannel k on dataflow link l is selected for flow f_i, and 0 otherwise. The variables $x_{i,k}^l$ allow us to schedule the RBs assigned to the flow while the variables $f_i^l.s$ are used to schedule the consecutive TTIs. The concept of the hyperperiod also applies to 5GS:

$$T_{5GS} = LCM(\{f_i.p | f_i \in F\}). \tag{11}$$

$f_i^l.o$, $f_i^l.s$ and $x_{i,k}^l$ for all flows on 5G dataflow links of its route $l \in p_i \cap L^{5GS}$ and each subchannel index $k \in \mathcal{F}$ are variables.

C. Trade-Off Between Bandwidth Usage and the 5GS Delay Budget

According to [32], non-deterministic traffic will coexist with deterministic TT traffic in the same slice, where non-deterministic traffic has no strict deadline for packets to be received and its typical use case is software updates or file download. We refer to such non-deterministic traffic as best-effort (BE) traffic. BE packets are transmitted in the intervals of TT flows. That is, the RBs for TT flows are pre-scheduled and reserved according to their 5G delay budget. The remaining RBs are used to transmit BE packets. In Fig. 6(a), TT flows f_1 and f_2 are represented as blue and green, respectively. The scheduling units for TT and BE packets are 2 and 5 TTIs, respectively. Thus, once a BE packet starts transmission on an RB, it occupies that RB for 5 consecutive TTIs. Note that although there are 8 resource blocks between the two successive green transmission instances, these blocks cannot be utilized by BE packets and are therefore wasted, because they span only 2 TTIs. This phenomenon of bandwidth waste caused by different scheduling units between TT traffic and BE traffic, has been reported in [11], [28]. The different scheduling units of TT traffic and BE traffic lead to a trade-off between 5GS frequency usage and 5GS delay budget allocated to TT traffic. The delay budget of a transmission instance is defined as the duration from the transmission of its first resource block to that of its last resource block. In Fig. 6(a), the delay budgets of the blue and green flows are 2 and 1 TTIs, respectively. Under this configuration, only 6 BE packets can be transmitted per hyperperiod. But if we relax the delay budget of green flow to 2 TTIs as shown in Fig. 6(b), we can transmit 12 BE packets in one hyperperiod and reduce bandwidth waste. Thus the delay budgets of TT flows can be traded for improved resource utilization in the 5GS.

D. Network Constraints

We now derive the constraints of the ATSM which accounts for both 5GS and TSN, and schedules flows from an e2e perspective. The constraints in Sections IV-D6, IV-D7, IV-D8, and IV-D9 are borrowed from the mature scheduling model in TSN [6], [28], but are modified, if needed, for the AAM.

1) Transmission-Opportunity Constraints: Every packet in 5GS cannot start its transmission until the start of a TTI, and the transmission time of a packet must be an integer multiple of TTI:

$$\forall l \in L^{5GS}, \forall f_i \in F:$$

$$\exists f_i^l \Rightarrow$$

$$f_i^l.o = c_i^l \times TTI \tag{12}$$

$$f_i^l.s = d_i^l \times TTI \tag{13}$$

Authorized licensed use limited to: University of Michigan Library. Downloaded on November 23,2026 at 18:04:37 UTC from IEEE Xplore. Restrictions apply.

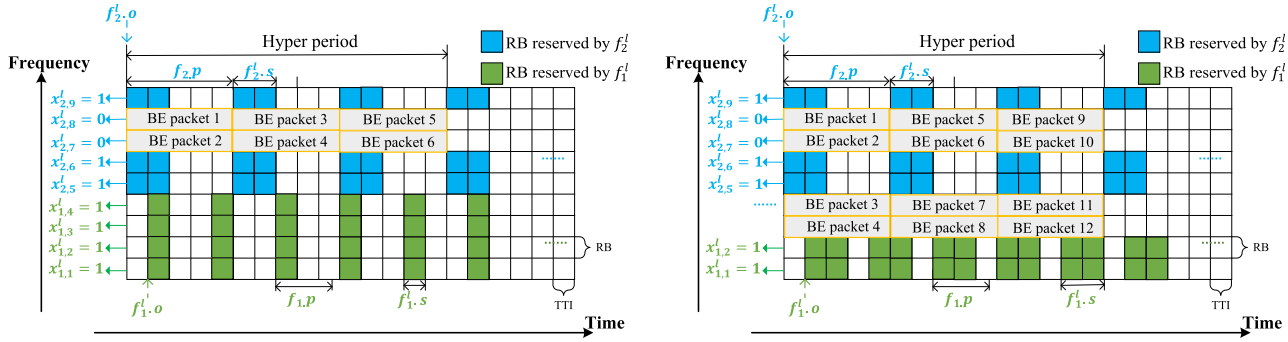

(a) Strict delay budget in 5GS.

(b) Relaxed delay budget in 5GS.

Fig. 6. Two TT flows' scheduling examples and trade-off between 5G delay budget and transmission number of BE packets. The green and blue colors represent the scheduling examples of the RBs of TT flows f_1 and f_2, respectively. (a) shows that 4 subchannels usage of green flow and 1 TTI delay budget for f_1 and 6 BE packets can be transmitted. (b) shows that 2 subchannel usage of green flow and the delay budget is relaxed as 2 TTI, 12 BE packets can be transmitted.

$$f_i^l.o + f_i^l.s \le f_i.p$$
$$c_i^l \in \left\{0, 1, \ldots, \left\lfloor \frac{f_i.p}{TTI} \right\rfloor - 1\right\}$$
$$d_i^l \in \left\{1, 2, \ldots, \left\lfloor \frac{f_i.p}{TTI} \right\rfloor\right\}. \quad (14)$$

where c_i^l denotes the TTI at which flow f_i begins transmission over the 5G dataflow link l and d_i^l is the number of consecutive TTIs occupied by the flow on the allocated RBs.

2) RB Constraints: We use binary variables y_k^l to indicate whether the k-th RB of 5G dataflow link l is scheduled to a flow. Specifically, $y_k^l = 1(0)$ if it is (not) assigned to a flow. So, we derive the following constraints:

$$\forall l \in L^{5GS}, \forall k \in \mathcal{F}, \exists f_i \in F:$$
$$x_{i,k}^l = 1 \Rightarrow y_k^l = 1. \quad (15)$$

If $y_k^l = 0$, all $x_{i,k}^l$ for all flows should be 0.

3) Resource Constraints: The resources allocated to a flow should be sufficient to transmit its packets. Let $R_{i,k}^l$ denote the number of bytes that can be transmitted by the k-th RB on the dataflow link l for the flow f_i, $R_{i,k}^l$ is used as a deterministic resource-planning input. It represents the transmission capability assumed during SPS scheduling, rather than the instantaneous stochastic wireless rate. Then, we have:

$$\forall l \in L^{5GS}, \forall f_i \in F:$$
$$\exists f_i^l \Rightarrow$$
$$\sum_{k=1}^{k_{\max}} x_{i,k}^l \times R_{i,k}^l \times d_i^l \ge f_i.l \quad (16)$$
$$\sum_{k=1}^{k_{\max}} x_{i,k}^l \times R_{i,k}^l \times (d_i^l - 1) < f_i.l$$
$$d_i^l \in \left\{1, 2, \ldots, \left\lfloor \frac{f_i.p}{TTI} \right\rfloor\right\} \quad (17)$$

If the actual wireless channel condition becomes worse than the estimated, the corresponding 5GS transmission may be delayed or retransmitted, which is evaluated in Figs. 8–10.

4) OFDMA Constraints: Any two flows cannot be assigned to the same TTI on the same frequency resource for f_1 and f_2 as shown in Fig. 5:

$$\forall l \in L^{5GS}, \forall f_i, f_j \in F, \forall k \in \mathcal{F},$$
$$\forall \alpha \in \left\{0, \ldots, \left\lfloor \frac{T_{5GS}}{f_i.p} \right\rfloor - 1\right\},$$
$$\forall \beta \in \left\{0, \ldots, \left\lfloor \frac{T_{5GS}}{f_j.p} \right\rfloor - 1\right\}:$$
$$((f_i \ne f_j) \wedge \exists f_i^l \wedge \exists f_j^l \wedge (x_{i,k}^l = 1) \wedge (x_{j,k}^l = 1))$$
$$\Rightarrow ((\alpha \times f_i.p) + f_i^l.o) \ge (\beta \times f_j.p) + f_j^l.o + f_j^l.s)$$
$$\vee ((\beta \times f_j.p) + f_j^l.o) \ge (\alpha \times f_i.p) + f_i^l.o + f_i^l.s). \quad (18)$$

5) Window Constraints: Potential transmission instances have the same period along the route of the flow, and the period should not be larger than that of the flow. Therefore,

$$\forall l \in L^{TSN}, \forall f_i \in F:$$
$$(\exists f_i^l \wedge (l \ne l_{h_i}))$$
$$\Rightarrow f_i^l.T = T_i \quad (19)$$
$$f_i^l.T \le f_i.p. \quad (20)$$

6) Frame Constraints: The offset must be nonnegative, and a potential transmission instance should finish the transmission within its period:

$$\forall l \in L^{TSN}, \forall f_i \in F:$$
$$(\exists f_i^l \wedge (l \ne l_{h_i}))$$
$$\Rightarrow f_i^l.o \ge 0 \quad (21)$$
$$f_i^l.o + f_i^l.s \le T_i. \quad (22)$$

7) Transmission Order Constraints: The transmission opportunity on the next wired dataflow link l_b should send the packet after it is fully received over the preceding wired dataflow link l_a:

$$\forall l_a, l_b \in L^{TSN}, \forall f_i \in F:$$

Authorized licensed use limited to: University of Michigan Library. Downloaded on November 23,2026 at 18:04:37 UTC from IEEE Xplore. Restrictions apply.

$$(\exists f_i^{l_a} \wedge \exists f_i^{l_b} \wedge isNextHop(l_b, l_a, f_i) \wedge (l_b \neq l_{h_i})) \Rightarrow f_i^{l_b}.o \geq f_i^{l_a}.o + f_i^{l_a}.s + ldelay^{l_a}, \quad (23)$$

where $ldelay^{l_a}$ is the propagation delay of the dataflow link l_a and function $isNextHop(l_b, l_a, f_i)$ returns true if l_b is the next dataflow link of l_a on the route of flow f_i else false.

8) TDMA Constraints: Wired links can only transmit one frame at a time, and hence potential transmission instances reserved for different flows should not overlap:

$$\begin{aligned}
&\forall l \in L^{TSN}, \forall f_i, f_j \in F,\\
&\forall \alpha \in \left\{0, \ldots, \left\lfloor \frac{T_{TSN}}{T_i} \right\rfloor - 1\right\},\\
&\forall \beta \in \left\{0, \ldots, \left\lfloor \frac{T_{TSN}}{T_j} \right\rfloor - 1\right\}:\\
&\quad ((f_i \neq f_j) \wedge \exists f_i^l \wedge \exists f_j^l \wedge (l \neq l_{h_i}) \wedge (l \neq l_{h_j}))\\
&\quad \Rightarrow ((\alpha \times T_i) + f_i^l.o\\
&\quad \geq (\beta \times T_j) + f_j^l.o + f_j^l.s)\\
&\quad \vee ((\beta \times T_j) + f_j^l.o\\
&\quad \geq (\alpha \times T_i) + f_i^l.o + f_i^l.s). \quad (24)
\end{aligned}$$

Note that T_i and T_j are variables which are different for the constants in the traditional scheduling of TSN. We will discuss how to linearize these constraints in Subsection IV-F.

9) Frame Isolation Constraints: If frames from different flows arrive simultaneously at the same TSN switch and share an output port, their queue order is non-deterministic [6]. So, only frames from the same flow can be stored in the queue:

$$\begin{aligned}
&\forall l_a, l_b, l_c \in L^{TSN}, \forall f_i, f_j \in F,\\
&\forall \alpha \in \left\{0, \ldots, \left\lfloor \frac{T_{TSN}}{T_i} \right\rfloor - 1\right\},\\
&\forall \beta \in \left\{0, \ldots, \left\lfloor \frac{T_{TSN}}{T_j} \right\rfloor - 1\right\}:\\
&((f_i \neq f_j)\\
&\wedge \exists f_i^{l_a} \wedge \exists f_i^{l_c} \wedge \exists f_j^{l_b} \wedge \exists f_j^{l_c}\\
&\wedge isNextHop(l_c, l_a, f_i)\\
&\wedge isNextHop(l_c, l_b, f_j)\\
&\wedge (l_c \neq l_{h_i}) \wedge (l_c \neq l_{h_j}))\\
&\Rightarrow (((\alpha \times T_i) + f_i^{l_c}.o\\
&\leq (\beta \times T_j) + f_j^{l_b}.o + ldelay^{l_b})\\
&\vee ((\beta \times T_j) + f_j^{l_c}.o\\
&\leq (\alpha \times T_i) + f_i^{l_a}.o + ldelay^{l_a}) \quad (25)
\end{aligned}$$

If f_i and f_j come from the same input port, l_a and l_b can be the same dataflow link.

10) e2e Delay Constraints: The e2e delay of a flow consists of 5GS and TSN parts. For the 5GS part, the delay is actually $f_i^{l_1}.s + T_{proc,gNB}$, where $T_{proc,gNB}$ is the (constant) processing delay of BS to receive packets. For TSN part, the delay is always fixed due to the AAM. It can be calculated using (2) in Section III-C. Thus, the e2e delay can be calculated by (3), and its elements that make up the formula are calculated as:

$$D_i^{5GS} = f_i^{l_1}.s + T_{proc,gNB} \quad (26)$$

$$D_{i,(1)}^{TSN} = (f_i^{l_{h_i-1}}.o + f_i^{l_{h_i-1}}.s + ldelay^{l_{h_i-1}}) - f_i^{l_2}.o \quad (27)$$

$$D_{i,(2)}^{TSN} = f_i^{h_i}.s + ldelay^{l_{h_i}}. \quad (28)$$

Eq. (26) gives the deterministic 5GS delay used in ATSM for resource planning. HARQ retransmissions and channel-induced transmission uncertainty are not modeled as random variables in the ATSM. Their impact is abstracted as extra 5G transmission jitter in Section V, as shown in Figs. 8–10. The e2e delay constraints can thus be described as:

$$\forall f_i \in F: \quad D_i^{e2e} = D_i^{5GS} + T_i + D_{i,(1)}^{TSN} + D_{i,(2)}^{TSN} \leq f_i.d. \quad (29)$$

E. Objective Function

In addition to the TT flows, many other types of traffic may coexist in an industrial setting. We need to reduce the resources used by TT flows and leave as much resources as possible for BE traffic.

For the 5GS part, we try to minimize the number of frequency-domain RBs assigned to TT flows, which is inspired by [33]. As shown in Fig. 6(a) and (b), a RB can be used by BE traffic if it is not occupied by TT flows. Thus, minimizing the frequency-domain resources of TT flows leaves more resources available for BE traffic:

$$\min \sum_{k \in \mathcal{F}} \frac{y_k}{|\mathcal{F}|}. \quad (30)$$

For the TSN part, due to the adoption of AAM, over-provisioned transmission opportunities will lead to unused transmission opportunities. Thus, in TSN, we aim to maximize the period of the transmission opportunities reserved for each flow to reduce resource overhead:

$$\max \sum_{f_i \in F} \frac{T_i}{f_i.p|F|}. \quad (31)$$

To obtain the final objective function, we multiply (31) by -1 to change the optimization direction, and then use a weighting factor γ to balance the two optimization objectives:

$$\min \left[\gamma \sum_{k \in \mathcal{F}} \frac{y_k}{|\mathcal{F}|} - (1-\gamma) \sum_{f_i \in F} \frac{T_i}{f_i.p \cdot |F|} \right]. \quad (32)$$

where $\gamma \in [0, 1]$ indicates which network we want to optimize more.

F. Problem Linearization

The ATSM proposed above can be transformed into an ILP problem. The "logical or" in (18), (24) and (25) and the product

Authorized licensed use limited to: University of Michigan Library. Downloaded on November 23,2026 at 18:04:37 UTC from IEEE Xplore. Restrictions apply.

of binary variable and bounded variable in (16) and (17) can be linearized by Big-M reformulations [34], [35] which are usually been a feature in optimization software such as Gurobi [36] and YALMIP [35]. But there still remains a difficulty: the number of constraints in (24) and (25) cannot be determined as the number is related to the T_i and T_j which are decision variables.

To overcome this difficulty, we adopt the following strategy:

- The minimum resource period that can be supported by TSN is denoted as $\min P$ whose unit is μs.
- For any flow f_i whose period is $f_i.p$, the available resource period T_i can only be selected from the list $list_i = [\min P, 2 \times \min P, 4 \times \min P, \ldots, T_{i,\max}]$ whose length is s_i and $T_{i,\max}$ satisfies:

$$T_{i,\max} = \min P \cdot 2^{s_i - 1} \tag{33}$$

$$\min P \times 2^{s_i - 1} \leq f_i.p \tag{34}$$

$$\min P \times 2^{s_i} > f_i.p. \tag{35}$$

- For any flow f_i, we introduce s_i binary variables $\{b_{i,j} | j = 0, 1, \ldots, s_i - 1\}$, and we let $T_i = \sum_{j=0}^{j=s_i-1} list_i[j] \times b_{i,j}$. Furthermore, we introduce new constraints to make only one element of the list can be selected:

$$\forall f_i \in F :$$

$$\sum_{j=0}^{j=s_i-1} b_{i,j} = 1. \tag{36}$$

In this way, the hyperperiod of the set $\mathbf{T}_{\max} = \{T_{i,\max} | f_i \in F\}$ is multiple of the hyperperiod of the set $\mathbf{T} = \{T_i | f_i \in F\}$. Then, we can expand the check range from $[0, \frac{T_{TSN}}{T_i} - 1]$ to $[0, \frac{LCM(\mathbf{T}_{\max})}{\min P} - 1]$ in (24) and (25). The optimization problem is transformed into an ILP problem. We use Gurobi [36] to solve the problem.

An ILP problem has exponential worst-case complexity with respect to the number of integer and binary decision variables. Let Γ denote the equivalent number of binary-encoded discrete variables in the linearized ILP, including binary variables and bounded integer variables. In the worst case, an exact solver may need to explore up to 2^{Γ} assignments. These variables include the 5GS RB assignment variables $x^l_{i,k}$, the RB-usage variables y^l_k, the TSN period selection variables $b_{i,j}$, and the integer variables used to determine transmission offsets and durations. Therefore, the model size grows with the number of flows, RBs, and candidate TSN transmission-opportunity periods. ATSM is not intended for highly dynamic per-packet online scheduling. It is suitable for scenarios where the flow set, periods, deadlines, and routes are known in advance or change slowly [29], [37]. For large-scale deployments, heuristic search can be used.

V. Performance Evaluation

We evaluate the performance of AAM and ATSM. All simulations are conducted with the discrete-event simulator OMNeT++ [20] with INET [39] and Simu5G [40] framework.

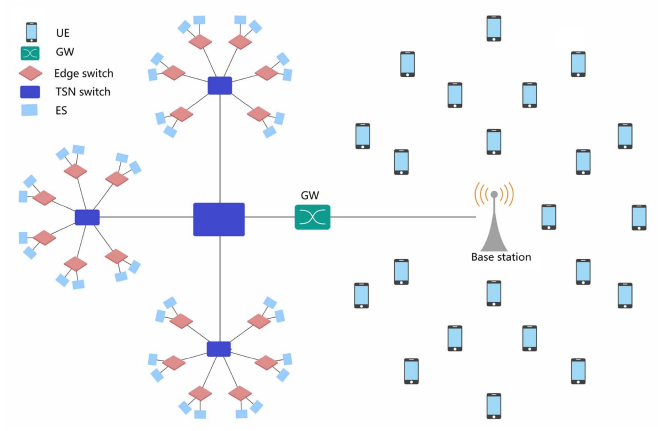

Fig. 7. Simulation topology of the integrated 5GS—TSN network.

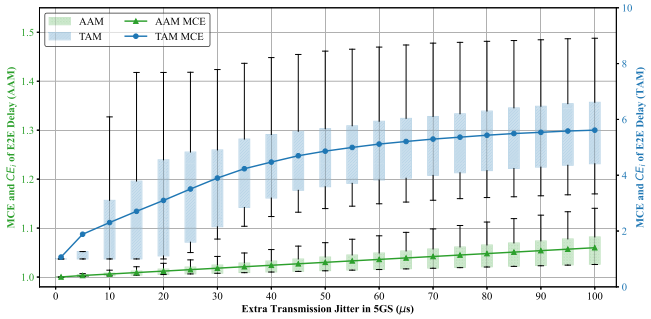

Fig. 8. CE_i and MCE of e2e delay for AAM-Scheduling and TAM-Scheduling under extra 5G transmission jitter.

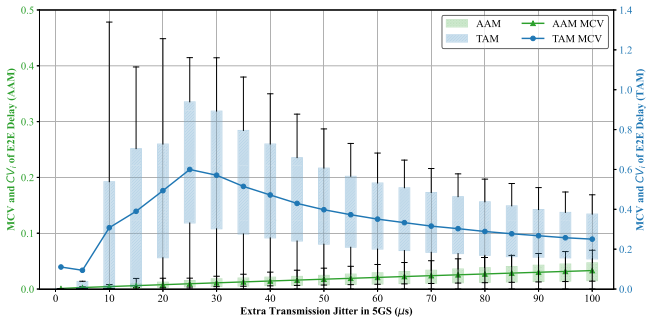

Fig. 9. CV_i and MCV of e2e delay for AAM-Scheduling and TAM-Scheduling under extra 5G transmission jitter.

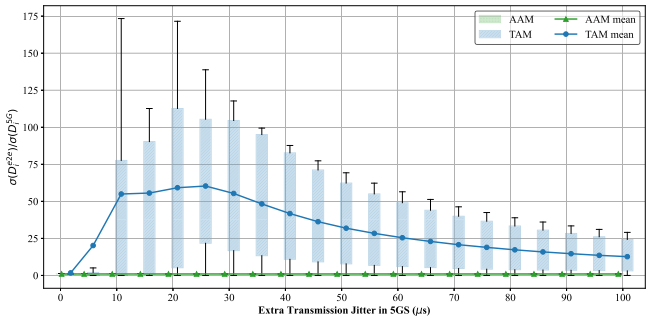

Fig. 10. The ratio of the standard deviation of e2e delay to the standard deviation of 5GS delay varies with extra 5G transmission jitter.

Authorized licensed use limited to: University of Michigan Library. Downloaded on November 23,2026 at 18:04:37 UTC from IEEE Xplore. Restrictions apply.

TABLE II
TEST CASES

Flow type	Period	Size	Delay	Rate (kbps)	Number of Flows
I	0.5 ms	96 B	0.5 ms	1536	5
II	1 ms	128 B	1 ms	1024	5
III	2 ms	256 B	2 ms	1024	10

TABLE III
SIMULATION PARAMETERS

Type	Parameter	Value
Wireless	Numerology	3
	Subcarrier spacing	120 kHz
	OFDM symbols per mini-slot	7
	Mini-slot duration	0.0625 ms
	$k_{\max}$	10
	$T_{\text{proc,gNB}}$	1 TTI
	Carrier frequency	3.8 GHz
	Channel model	Urban Macrocell according to [38]
Wired	Data rate	100 Mbps
	Propagation delay	1 μs
	$minP$	100 μs

A. Simulation Setup

The topology of the simulation network is shown in Fig. 7, which is based on the medium-sized topology presented in [6] and is extended with 5GS. There are 36 ESs in TSN and 20 UEs uniformly distributed around the BS in 5GS. The traffic types and their configurations are summarized in Table II. Each UE serves as the source of one flow, whose destination is randomly selected from the set of ESs in TSN. The last column of Table II denotes the number of flows of each traffic type used in Section V-B. The remaining simulation parameters are summarized in Table III.

Algorithm 1 and Algorithm 2 of AAM are implemented at the GW and edge switch, respectively. The configurations of 5GS, TSN switches, GW and edge switch are calculated using the model presented in Section IV.

B. Evaluation of AAM

1) Comparison With TAM: In the first set of experiments, we evaluate the performance of AAM compared to TAM in the presence of the 5G transmission jitter and the clock skew between the two systems. To distinguish between different experiments, we name the experiment conducted by ATSM proposed in Section IV as the *AAM-Scheduling*. The baseline is called the *TAM-Scheduling*, which uses a scheduling model called the *synchronous traffic scheduling model* (STSM). The STSM is modified from the ATSM by not applying the AAM, i.e., the period of the potential transmission instances equals to the flow period, the packets have to arrive at the GW before the start of their preassigned transmission opportunities, and no packet-holding process is applied, as in [28].

We collect e2e delay of each packet of flow f_i and calculate mean and standard deviation of them denoted as $\bar{D}^{e2e}_{i,Actual}$ and $\sigma(D^{e2e}_i)$. As shown in (37) and (38), we use the coefficient of expansion (CE) and coefficient of variation (CV) of the e2e delay to evaluate the ratios of e2e delay enlargement and e2e jitter, respectively. CE is defined as the ratio of the mean actual e2e delay to the scheduled delay and CV is defined as the ratio of the standard deviation of the e2e delay to the mean actual e2e delay:

$$\forall f_i \in F:$$

$$CE_i = \frac{\bar{D}^{e2e}_{i,Actual}}{D^{e2e}_{i,Scheduled}} \tag{37}$$

$$CV_i = \frac{\sigma(D^{e2e}_i)}{\bar{D}^{e2e}_{i,Actual}}, \tag{38}$$

where $D^{e2e}_{i,Scheduled}$ is the e2e delay calculated by the scheduling model, which assume no transmission jitter in 5GS, $\bar{D}^{e2e}_{i,Actual}$ is the mean e2e delay the packets actually experience under transmission jitter in 5GS, and $\sigma(\cdot)$ is the standard deviation calculated by accounting for the e2e delay of each packet.

Then, the mean coefficient of expansion (MCE) and the mean coefficient of variation (MCV) are calculated to evaluate the ratios of e2e delay enlargement and jitter of the whole system, respectively:

$$MCE = \sum_{f_i \in F} \frac{CE_i}{|F|} \tag{39}$$

$$MCV = \sum_{f_i \in F} \frac{CV_i}{|F|}. \tag{40}$$

Performance with 5G Transmission Jitter: We first assume 5GS and TSN are synchronized and introduce an extra transmission jitter in 5GS. Specifically, we vary the extra transmission jitter from 0 μs to 100 μs with step 5 μs by introducing a random extra delay for each packet in 5GS, and the extra delay follows a uniform distribution. For example, if the extra transmission jitter is 10 μs, the introduced extra delay for each packet is sampled from the uniform distribution $U(0\ \mu\text{s}, 10\ \mu\text{s})$. At each value of the extra transmission jitter, we collect the e2e delay of each packet of flow f_i and calculate its CE_i. We also calculate MCE and MCV according to (39) and (40). The distribution of CE_i is visualized using box plots for different values of the extra transmission jitter. The results are shown in Fig. 8. The MCE is also depicted in the same figure using a dashed line.

In Fig. 8, the MCE of the e2e delay of the TAM-Scheduling increases rapidly as the extra transmission jitter increases, since more packets will miss their corresponding transmission opportunities and a missed transmission opportunity incurs an additional waiting delay as shown in Fig. 2(b). In contrast, the MCE of the AAM-Scheduling increases very slowly compared to that of the TAM-Scheduling because missing a transmission opportunity has no impact on the constant delay in TSN as shown in Fig. 2(d) and (2). The e2e delay only scales with the delay in 5GS which is affected by the extra transmission jitter. Thus, the delay enlargement is significantly mitigated by the AAM, which is consistent with Fig. 2(d). For the same reasons, CE_i of TAM is widely dispersed while the corresponding indicators for AAM remain within a much narrower range.

Fig. 9 shows the boxplots of CV_i and the dashed lines of MCV for TAM-Scheduling and the AAM-Scheduling. Fig. 10 shows the boxplots of the ratio of the standard deviation of e2e delay to the standard deviation of 5GS delay, together with their corresponding averages shown by dashed lines. In these two

Authorized licensed use limited to: University of Michigan Library. Downloaded on November 23,2026 at 18:04:37 UTC from IEEE Xplore. Restrictions apply.

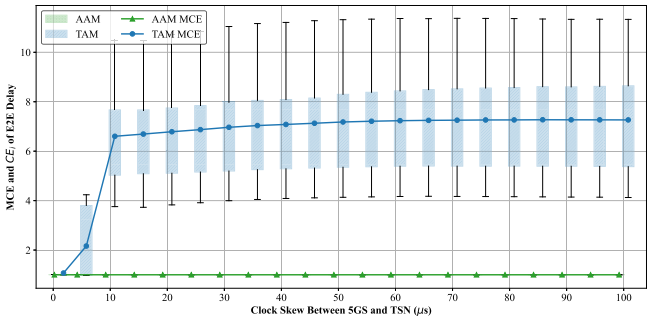

Fig. 11. CE_i and MCE of e2e delay for AAM-Scheduling and TAM-Scheduling with clock skew between 5GS and TSN.

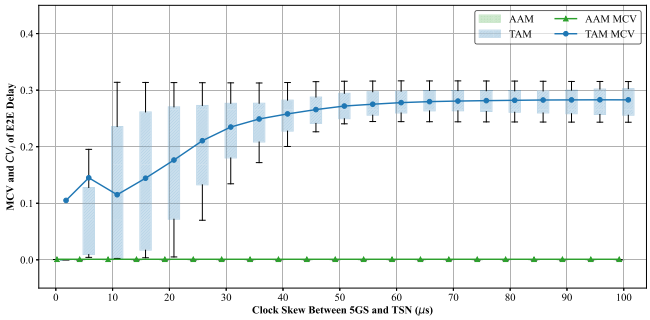

Fig. 12. CV_i and MCV of e2e delay for AAM-Scheduling and TAM-Scheduling with clock skew between 5GS and TSN.

figures, the curves of the TAM-Scheduling first increase rapidly, because more packets miss their transmission opportunities as the extra transmission jitter increases. And then they will decrease after the peak because more packets are transmitted in the next transmission opportunities in their next flow periods, thus decreasing the e2e jitter. However, the MCV of the AAM-scheduling increases much more slowly than that of the TAM-Scheduling, and the ratio of the standard deviation of the e2e delay to the standard deviation of 5GS delay remains equal to 1 for AAM as shown in Fig. 10. This is because the transmission delay in TSN is constant and the e2e jitter is only contributed by the 5G transmission jitter. Consequently, AAM significantly mitigates jitter amplification. Furthermore, we can see the results of AAM scatter within a small range while the results of TAM scatter in a broader range.

Performance under Clock Skew: To evaluate the impact of clock skew between 5GS and TSN, we keep the 5G transmission jitter fixed and introduce different clock skew between the two systems. Specifically, the clock skew is changed from 0 μs to 100 μs with step 5 μs and the clock deviation follows a uniform distribution. For example, if the clock skew equals $5us$, the deviation between the clocks of TSN and 5GS is sampled from the uniform distribution $U(-2.5us, 2.5us)$. The positive deviation indicates that the TSN clock is ahead of the 5GS clock, and vice versa. The experiment results are shown in Figs. 11 and 12.

As shown in Fig. 11, the MCE of the TAM-Scheduling increases as the clock skew increases, consistent with the situations shown in Fig. 2(a). And the MCE of the AAM-Scheduling is fixed which is consistent with the situation shown in Fig. 2(c).

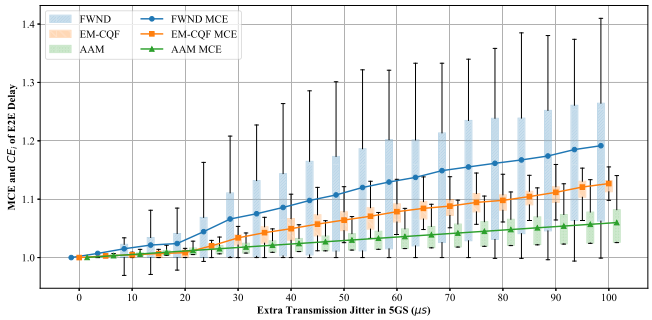

Fig. 13. CE_i and MCE of e2e delay for AAM, FWND, and EM-CQF under extra 5G transmission jitter.

Fig. 12 shows similar results. In particular, the results of AAM almost keep at a constant while the results of TAM are widely scattered over a large range in these two figures. These results demonstrate the AAM can significantly mitigate the delay and jitter enlargement caused by the clock skew between the two systems.

2) Comparison With TSN-Side Asynchronous Methods: We further compare AAM with two representative TSN-side methods that can tolerate uncertain ingress traffic [41] [42]. The packets output by 5GS can be regarded as asynchronous ingress traffic to the TSN domain. Barzegaran et al. [41] proposed a flexible window-based GCL method (FWND), which addresses asynchronous arrivals by enlarging precise transmission instants into flexible sending windows. A packet arriving within a sending window can contend for transmission according to priority, whereas a packet missing the current window has to wait for a later window. Therefore, the delay variation of FWND comes from both the in-window contention delay and the waiting delay caused by missed windows. To provide timing guarantees under such non-deterministic queue states, FWND derives the worst-case queueing delay based on the backlog bound at each output port. Yang et al. [42] enhanced the original cyclic queueing and forwarding (CQF) to multiple cyclic queues (EM-CQF). When a packet cannot be accommodated by the current sending queue, it can be stored in another cyclic queue and waits until the corresponding transmission cycle becomes active. This design improves the tolerance of CQF to uncertain sending times, but the forwarding delay is still coupled with the configured cycle length and the assigned queuing offset. In our implementation, the number of cyclic queues in EM-CQF is set to three. The extra 5G transmission jitter is varied from 0 μs to 100 μs with a step of 5 μs.

Figs. 13 and 14 show the e2e delay distortion under different levels of extra 5G transmission jitter. As the 5G transmission jitter increases, FWND exhibits the largest growth in both MCE and MCV. This is because the packets output by 5GS may arrive at different positions within a sending window or even miss the current window. In the former case, multiple packets may contend for transmission within the same window; in the latter case, the packet has to wait for a later window. Both increase the e2e delay and its variation. EM-CQF performs better than FWND because multiple cyclic queues and queuing offsets provide more regular forwarding opportunities for packets with

Authorized licensed use limited to: University of Michigan Library. Downloaded on November 23,2026 at 18:04:37 UTC from IEEE Xplore. Restrictions apply.

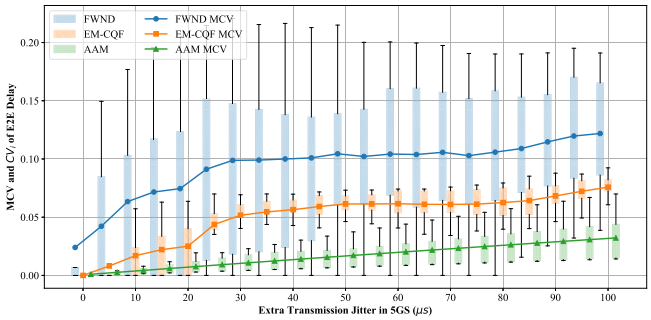

Fig. 14. CV_i and MCV of e2e delay for AAM, FWND, and EM-CQF under extra 5G transmission jitter.

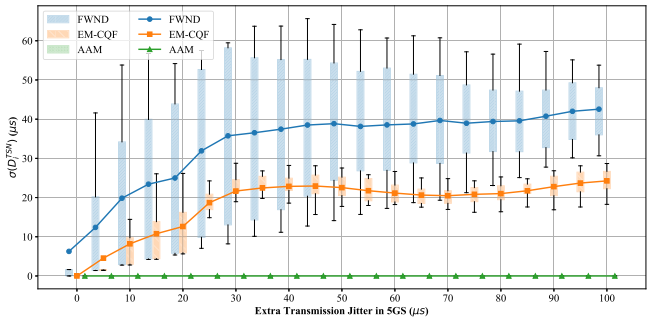

Fig. 15. The standard deviation of TSN delay for AAM, FWND, and EM-CQF under extra 5G transmission jitter.

uncertain arrival times. However, EM-CQF is still a cycle-based forwarding mechanism. Once a packet cannot be forwarded in its expected cycle, it has to wait until the corresponding queue becomes active in a later cycle. Unlike FWND and EM-CQF, AAM does not only make TSN forwarding more tolerant to uncertain ingress traffic but also reshapes the residence time in TSN by coupling the waiting time at the GW with the holding time at the edge switch. The redundant transmission opportunities at the GW reduce the waiting delay due to missed opportunities, while the holding process compensates for the variable waiting time before the packet leaves TSN. Therefore, the delay variation introduced by 5GS is not amplified any further by the TSN gate schedules.

Fig. 15 further verifies this observation from the perspective of TSN delay. With the increase of extra 5G transmission jitter, both FWND and EM-CQF introduce non-negligible standard deviations in the TSN delay. This indicates that the uncertainty at the 5GS output still propagates into the TSN domain. In contrast, AAM keeps $\sigma(D_i^{TSN})$ equal to zero for all tested jitter bounds. This result directly confirms that AAM isolates the transmission uncertainty within 5GS and eliminates the jitter amplification in TSN.

C. Evaluation of ATSM

In the second set of experiments, we evaluate the performance of the ATSM in the resource assignment under different traffic loads and optimization preferences. All flows have the same parameters: the packet length is $200B$, and both the period and the delay requirement are set to 1 ms. Different traffic loads are

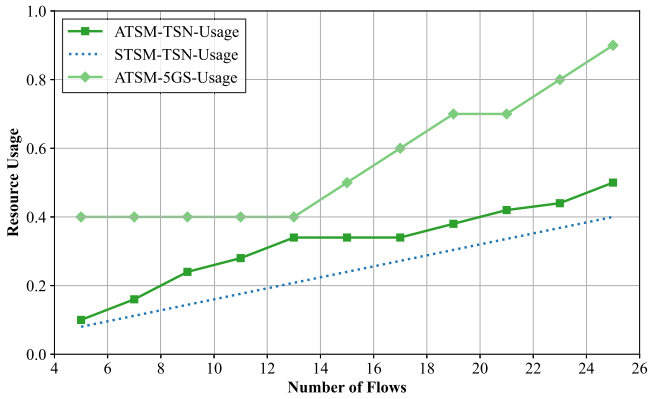

Fig. 16. TSN and 5GS resource usage scheduled by the ATSM with different numbers of flows.

generated by varying the number of flows. Different optimization preferences are represented by adjusting the parameter γ.

We then calculate TSN resource usage and 5GS resource usage, where 5GS resource usage is defined as the ratio of the frequency-domain resources allocated to TT flows to the total frequency-domain resources in 5GS. In addition to the two types of resource usage of the ATSM, the TSN resource usage of the STSM is also computed to represent the theoretical lower bound on the TSN resource usage that can be achieved by ATSM.

1) Performance Under Different Traffic Loads: First, the number of flows is changed from 5 to 25 with steps of 2, while other parameters are fixed and $\gamma = 0.5$. Multiple flows may originate from the same UE when the number of flows exceeds 20. The relevant results are shown in Fig. 16.

In Fig. 16, we can see resource usage of 5GS remains flat when flow number is no more than 13 and it begins to increase once the number of flows exceeds 13, while usage of TSN consistently increases as the number of flows increases. The reasons are as follows: (a) When the number of flows is 5, in order to satisfy e2e deadline, as shown in the Fig. 6(a), the scheduler allocates enough RBs to transmit packets of these flows, resulting in a large number of idle RBs between packets of these periodic flows. (b) As the number of flows increases from 5 to 13, the additional TT transmissions can be assigned to the same activated subchannel set at different non-overlapping TTIs. (c) When the number of flows exceeds 13, the RBs allocated have been fully occupied in different TTIs and no idle RBs are available. As a result, the scheduler has to use new subchannels to meet the demand of the newly added flows, causing the 5GS resource usage to increase with the number of flows. Fig. 16 also shows TSN usage of STSM. The gap between ATSM-TSN-Usage and STSM-TSN-Usage is the over-provisioning usage of ATSM.

2) Performance Under the Different Optimization Preferences: We now change the γ from 0 to 1 with step size $= 0.1$ and fix the number of flows at 10. The relevant results are shown in Fig. 17.

The trend of the two curves is that as γ increases, the 5GS resources usage decreases while the TSN resource usage increases. When γ changes from 0 to 0.1, the 5GS resource usage exhibits a sharp decrease since the ATSM starts to take care of it

Authorized licensed use limited to: University of Michigan Library. Downloaded on November 23,2026 at 18:04:37 UTC from IEEE Xplore. Restrictions apply.

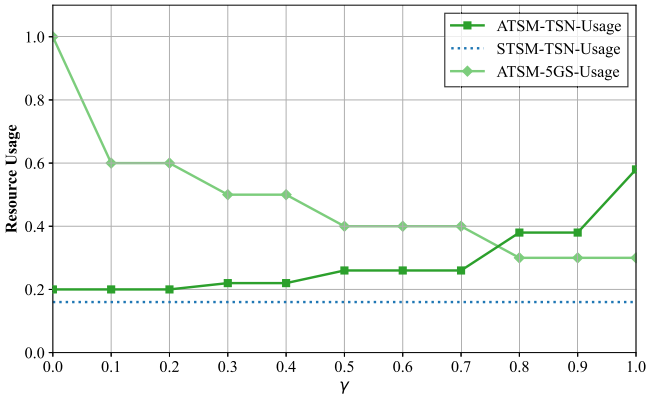

Fig. 17. TSN and 5GS resource usage scheduled by the ATSM with different γ.

which is illustrated in (32), and an opposite phenomenon occurs to the TSN resource usage when γ changes from 0.9 to 1. Then, TSN-Usage and 5GS-Usage gradually increase and decrease, and the absolute slope of TSN-Usage is smaller than that of 5GS-Usage curve. This is because the linearization method introduced in Section IV-F provides little room for the ATSM to optimize the TSN-Usage, whereas the 5GS-Usage can be optimized more effectively. The ATSM can thus use γ to apply different optimization preferences. A larger γ is suitable when 5GS radio resources are scarce or when more radio resources should be preserved for BE traffic. A smaller γ is suitable when TSN bandwidth or gate-control resources are the bottleneck. If neither domain is preferred, γ=0.75 provides a balanced setting in our evaluated scenarios.

VI. Conclusion

To mitigate the delay and jitter enlargement when 5GS and TSN are integrated by TAM, we have presented a new mechanism, AAM, for this integration. With this mechanism, the jitter of the transmission is isolated only in 5GS and the delay of packets in TSN can be kept constant. To coordinate the allocation of resources in the converged network, we have then proposed a scheduling model called ATSM based on the AAM. Finally, the superior performance of the AAM and the ATSM have been corroborated via simulation using the OMNeT++ simulator. As the AAM over-provisions resources to ensure the deterministic transmission of the traffic from 5GS to TSN, in future, we will consider how to dynamically utilize the allocated but un-utilized resources effectively.

References

[1] M. Wollschlaeger, T. Sauter, and J. Jasperneite, "The future of industrial communication: Automation networks in the era of the Internet of Things and industry 4.0," *IEEE Ind. Electron. Mag.*, vol. 11, no. 1, pp. 17–27, Mar. 2017.

[2] J. Jin et al., "Cloud-fog automation: The new paradigm toward autonomous industrial cyber-physical systems," *IEEE J. Sel. Areas Commun.*, vol. 43, no. 9, pp. 2917–2937, Sep. 2025.

[3] C.von Arnim, M. Dragan, F. Frick, A. Lechler, O. Riedel, and A. W. Verl, "TSN-based converged industrial networks: Evolutionary steps and migration paths," in *Proc. 25th IEEE Int. Conf. Emerg. Technol. Factory Automat.*, 2020, pp. 294–301.

[4] M. Gundall, C. Glas, and H. D. Schotten, "Feasibility study on virtual process controllers as basis for future industrial automation systems," in *Proc. 22nd IEEE Int. Conf. Ind. Technol.*, 2021, pp. 1080–1087.

[5] "Industrial ethernet is now bigger than fieldbuses," 2018. [Online]. Available: https://www.hms-networks.com/news-and-insights/news-from-hms/2018/02/27/industrial-ethernet-is-now-bigger-than-fieldbuses

[6] M. L. Raagaard and P. Pop, "Optimization algorithms for the scheduling of IEEE 802.1 time-sensitive networking (TSN)," 2018. [Online]. Available: https://api.semanticscholar.org/CorpusID:245903753

[7] L.-M. Deng, G. Xie, H. Liu, Y. Han, R. Li, and K. Li, "A survey of real-time ethernet modeling and design methodologies: From AVB to TSN," *ACM Comput. Surv.*, vol. 55, pp. 1–36, 2022.

[8] "Time-sensitive networking task group," 2023. [Online]. Available: https://www.ieee802.org/1/pages/tsn.html

[9] L. L. L. Bello and W. Steiner, "A perspective on IEEE time-sensitive networking for industrial communication and automation systems," *Proc. IEEE*, vol. 107, no. 6, pp. 1094–1120, Jun. 2019.

[10] M. Khoshnevisan, V. Joseph, P. K. Gupta, F. Meshkati, R. Prakash, and P. Tinnakornsrisuphap, "5G industrial networks with CoMP for URLLC and time sensitive network architecture," *IEEE J. Sel. Areas Commun.*, vol. 37, no. 4 pp. 947–959, Apr. 2019.

[11] D. Ginthör, J. von Hoyningen-Huene, R. Guillaume, and H. D. Schotten, "Analysis of multi-user scheduling in a TSN-enabled 5G system for industrial applications," in *Proc. IEEE Int. Conf. Ind. Internet*, 2019, pp. 190–199.

[12] M. K. Atiq, R. Muzaffar, Ó. Seijo, I. Val, and H.-P. Bernhard, "When IEEE 802.11 and 5G meet time-sensitive networking," *IEEE Open J. Ind. Electron. Soc.*, vol. 3, pp. 14–36, 2022.

[13] P. Kehl et al., "Prototype of 5G integrated with TSN for edge-controlled mobile robotics," *Electronics*, vol. 11, 2022, Art. no. 1666.

[14] F. Hamidi-Sepehr et al., "5G URLLC: Evolution of high-performance wireless networking for industrial automation," *IEEE Commun. Standards Mag.*, vol. 5, no. 2, pp. 132–140, Jun. 2021.

[15] 3rd Generation Partnership Project (3GPP), "Technical specification group services and system aspects; study on communication for automation in vertical domains(release 16)," 3GPP, Sophia Antipolis, France, Tech. Rep. 22.804, 2018.

[16] M. Adil, T. Qiu, X. Zhou, D. Javeed, Z. Cao, and D. Oliver Wu, "Integrated 5G and time sensitive networking for emerging applications: A survey of advancements, challenges, and future directions," *IEEE Commun. Surveys Tuts.*, vol. 28, pp. 4016–4050, 2026.

[17] 3rd Generation Partnership Project (3GPP), "System architecture for 5G system (release 17)," 3GPP, Sophia Antipolis, France, Tech. Specification 23.501, 2023.

[18] Z. ZhuYan, S. Jun, and L. Jun, "Deterministic communications in edge AI: 5G-TSN integration solutions and implementation," in *Proc. IEEE 23rd Int. Conf. Ind. Inform.*, 2025, pp. 1–6.

[19] P. Rodriguez-Martin, O. Adamuz-Hinojosa, P. Muñoz, J. Caleya-Sanchez, J. Navarro-Ortiz, and P. Ameigeiras, "Empirical analysis of the impact of 5G jitter on time-aware shaper scheduling in a 5G-TSN network," in *Proc. IEEE 21st Int. Conf. Factory Commun. Syst.*, 2025, pp. 1–8.

[20] "OMNeT discrete event simulator," 2023. [Online]. Available: https://omnetpp.org/

[21] C. Singhal and S. De, *Resource Allocation in Next-Generation Broadband Wireless Access Networks*. New York, NY, USA: IGI Glob., 2017.

[22] A. Larrañaga, M. C. Lucas-Estañ, I. Martinez, and J. Gozálvez, "5G configured grant scheduling for 5G-TSN integration for the support of industry 4.0," *Proc. 18th Wireless On-Demand Netw. Syst. Serv. Conf.*, 2023, pp. 72–79.

[23] Y. Cai, X. Zhang, S. Hu, and X. Wei, "Dynamic QoS mapping and adaptive semi-persistent scheduling in 5G-TSN integrated networks," *China Commun.*, vol. 20, pp. 340–355, Apr. 2023.

[24] S. R. B. Da Silva, F. G. Vogt, F. R. Cesen, M. C. Luizelli, C. E. Rothenberg, and G. Patra, "Bridging TSN and 5G: Synchronization and flow mapping for smart manufacturing," in *Proc. IEEE 11th Int. Conf. Netw. Softwarization*, 2025, pp. 91–96.

[25] J. Yang and G. Yu, "Traffic scheduling for 5G-TSN integrated systems," in *Proc. Int. Symp. Wireless Commun. Syst.*, 2022, pp. 1–6.

[26] X. Wang, H. Yao, T. Mai, S. Guo, and Y. Liu, "Reinforcement learning-based particle swarm optimization for end-to-end traffic scheduling in TSN-5G networks," *IEEE/ACM Trans. Netw.*, vol. 31, no. 6, pp. 3254–3268, Dec. 2023.

[27] M. Li, S. Guo, C. Chen, C. Chen, X. Liao, and X. Guan, "DecAge: Decentralized flow scheduling for industrial 5G and TSN integrated networks," *IEEE Trans. Netw. Sci. Eng.*, vol. 11, no. 1, pp. 543–555, Jan./Feb. 2023.

Authorized licensed use limited to: University of Michigan Library. Downloaded on November 23,2026 at 18:04:37 UTC from IEEE Xplore. Restrictions apply.

[28] D. Ginthör, R. Guillaume, J. von Hoyningen-Huene, M. Schüngel, and H. D. Schotten, "End-to-end optimized joint scheduling of converged wireless and wired time-sensitive networks," *Proc. 25th IEEE Int. Conf. Emerg. Technol. Factory Automat.*, 2020, pp. 222–229.
[29] W. Steiner, "An evaluation of SMT-based schedule synthesis for time-triggered multi-hop networks," in *Proc. 31st IEEE Real-Time Syst. Symp.*, 2010, pp. 375–384.
[30] T. Zhang, F. Jiaqi, Y. Ma, S. Qu, and F. Ren, "Survey on traffic scheduling in time-sensitive networking," *J. Comput. Res. Develop.*, vol. 59, no. 4, pp. 747–764, 2022.
[31] D. Jiang, H. Wang, E. M. Malkamaki, and E. Tuomaala, "Principle and performance of semi-persistent scheduling for VoIP in LTE system," *Proc. Int. Conf. Wireless Commun. Netw. Mobile Comput.*, 2007, pp. 2861–2864.
[32] J. García-Morales, M. C. Lucas-Estañ, and J. Gozálvez, "Latency-sensitive 5G RAN slicing for industry 4.0," *IEEE Access*, vol. 7, pp. 143139–143159, 2019.
[33] G. Karadag, R. Gul, Y. Sadi, and S. C. Ergen, "QoS-constrained semi-persistent scheduling of machine-type communications in cellular networks," *IEEE Trans. Wireless Commun.*, vol. 18, no. 5, pp. 2737–2750, May 2019.
[34] F. Trespalacios and I. E. Grossmann, "Improved Big-M reformulation for generalized disjunctive programs," *Comput. Chem. Eng.*, vol. 76, pp. 98–103, 2015.
[35] "Big-M reformulations," 2024. [Online]. Available: https://yalmip.github.io/tutorial/bigmandconvexhulls
[36] Gurobi Optimization, LLC, "Gurobi optimizer reference manual," 2022. [Online]. Available: https://www.gurobi.com
[37] R. Serna Oliver, S. S. Craciunas, and W. Steiner, "IEEE 802.1 Qbv gate control list synthesis using array theory encoding," in *Proc. IEEE Real-Time Embedded Technol. Appl. Symp.*, 2018, pp. 13–24.
[38] 3rd Generation Partnership Project (3GPP), "Study on channel model for frequencies from 0.5 to 100GHz (release 17)," 3GPP, Sophia Antipolis, France, Tech. Rep. 38.901, 2022.
[39] "INET framework," 2023. [Online]. Available: https://inet.omnetpp.org/
[40] G. Nardini, D. Sabella, G. Stea, P. Thakkar, and A. Virdis, "Simu5G–An OMNeT++ library for end-to-end performance evaluation of 5G networks," *IEEE Access*, vol. 8, pp. 181176–181191, 2020.
[41] M. Barzegaran, N. Reusch, L. Zhao, S. S. Craciunas, and P. Pop, *Real-Time Traffic Guarantees in Heterogeneous Time-Sensitive Networks*, New York, NY, USA: Assoc. Comput. Machinery, 2022, pp. 46–57, doi: 10.1145/3534879.3534921.
[42] D. Yang, Z. Cheng, W. Zhang, H. Zhang, and X. Shen, "Burst-aware time-triggered flow scheduling with enhanced multi-CQF in time-sensitive networks," *IEEE/ACM Trans. Netw.*, vol. 31, no. 6, pp. 2809–2824, Dec. 2023.



Jiamin Cui received the BS degree in computer science and technology from the College of Computer Science and Technology, Taiyuan University of Technology, Taiyuan, China, in 2025. She is currently working toward the MS degree with Beijing Jiaotong University. Her research interests include time-sensitive networks and time synchronization.



Jiacheng Li received the BS degree in telecommunication engineering in 2021 from the School of Electronic and Information Engineering, Beijing Jiaotong University, Beijing, China, where he is currently working toward the MS degree. His research interests include industrial real-time networking and traffic scheduling.



Yongxiang Zhao received the PhD degree in electrical engineering from Beijing Jiaotong University (BJTU), Beijing, China, in 2002. He is currently an associate professor with the School of Electronic and Information Engineering, BJTU. His research interests include network protocol and algorithm design, quality of video streaming, and modeling and design of communication networks.



Chunxi Li received the BS degree in telecommunication engineering, and the MS and PhD degrees in communication and information systems from Beijing Jiaotong University (BJTU), Beijing, China, in 1992, 1997, and 2010, respectively. He is currently an associate professor with the School of Electronic and Information Engineering, BJTU. His research interests include measurement and modeling on online mobile streaming systems, distributed caching network, and industrial traffic scheduling.



Zonghui Li (Member, IEEE) received the BS degree in computer science from Beijing Information Science and Technology University in 2010, and the MS and PhD degree from the Institute of Microelectronics and School of Software, Tsinghua University, Beijing, China, in 2014 and 2019, respectively. He is currently an associate professor with the School of Computer and Information Technology, Beijing Jiaotong University, Beijing, China. His research interests include embedded and high performance computing, real-time embedded systems, especially for industrial control networks, and fog computing.



Kang G Shin (Life Fellow, IEEE) received the BS degree in electronics engineering from Seoul National University, Seoul, Korea, and the MS and PhD degrees in electrical engineering from Cornell University, Ithaca, New York, in 1970, 1976, and 1978, respectively. He is currently the Kevin & Nancy O'Connor professor of computer science with the Department of Electrical Engineering and Computer Science, The University of Michigan, Ann Arbor. He has supervised the completion of 93 PhDs and authored/coauthored close to 1,000 technical articles, textbook and about 60 patents or invention disclosures. His research interests include QoS-sensitive computing and networking and on embedded real-time and cyber-physical systems. He was the recipient of received numerous awards, including the 2022 IEEE Computer Society Technical & Conference Activities Board Distinguished Leadership Award in real-time systems. He is also an ACM fellow.



Bo Ai (Fellow, IEEE) received the master's degree and PhD degrees from Xidian University in China. He was an excellent postdoctoral research fellow with Tsinghua University in 2007. He was a visiting professor with EE Department, Stanford University in 2015. He is currently with a full professor and PhD candidate advisor with Beijing Jiaotong University. He is also the deputy director of the State Key Lab of Rail Traffic Control and Safety and International Joint Research Center. He has authored/co-authored eight books and more than 300 academic research papers in his research interests. He has hold 26 invention patents. He is a Fellow of the Institution of Engineering and Technology (IET Fellow) and IEEE VTS distinguished lecturer. He was the recipient of many awards including Distinguished Youth Foundation and Excellent Youth Foundation from National Natural Science Foundation of China.

Authorized licensed use limited to: University of Michigan Library. Downloaded on November 23,2026 at 18:04:37 UTC from IEEE Xplore. Restrictions apply.